THE ASTROPHYSICAL JOURNAL, 457:L47–L50, 1996 January 20


# NON-LTE EFFECTS IN AMMONIA

R. A. GAUME,[1] T. L. WILSON,[2,3] AND K. J. JOHNSTON[1]
*Received 1995 June 20; accepted 1995 November 3*


## ABSTRACT

The non-LTE effects in the $NH_3$ $(J,K) = (1, 1)$ absorption toward the DR 21 H II region have been investigated using a spatial resolution of 1.″7–3″. The anomalies, found in the satellite hyperfine (HF) components, indicate significant, widespread departures from LTE. We present images of the LTE departure for the inner and outer pairs of $NH_3$ (1, 1) HF components toward the H II region and find, surprisingly, that the degree of LTE departure for these HF components is spatially *anticorrelated*. Previous models predicted a spatial correlation. This unexpected result may be explained by a dynamic model involving both the infall and outflow of molecular material. Although weak emission in the redshifted outer HF component is widespread toward the continuum, an unresolved, high brightness temperature ($\geq$600 K) maser is found just southwest of the continuum peak. This is the first proven instance of an interstellar maser in the $NH_3$ (1, 1) level. The flux density of the maser is larger than the absolute value of the flux density of any of the other HF components (seen in absorption), including the main component.


*Subject headings:* ISM: clouds — ISM: individual (DR 21) — ISM: molecules — masers — molecular data — molecular processes — radio lines: ISM

## 1. INTRODUCTION

$NH_3$ is a symmetric-top molecule; a general discussion of the structure is contained in Townes & Schawlow (1955). A schematic energy-level diagram of the $(J,K) = (2, 1)$ and (1, 1) levels is shown in Figure 1. Each $(J,K)$ level of $NH_3$ is split into a doublet level. The centimeter-wavelength lines of $NH_3$ are caused by transitions between the upper and lower states of a particular doublet level. The centimeter lines are again split by hyperfine (HF) interactions into a main HF component and two pairs of satellite HF components symmetrically placed about the main component. Under conditions of LTE, one expects the individual components of a satellite HF pair to have equal intensity.

It has been known for some time that the satellite HF components of $NH_3$ exhibit non-LTE effects in certain interstellar regions. The first example of this effect was found in the absorption spectrum of $NH_3$ toward the H II region DR 21 (Wilson & Pauls 1980; Matsakis et al. 1977). Anomalies have been subsequently found in the emission spectra toward several other regions of star formation (see, e.g., Stutzki, Ungerechts, & Winnewisser 1982; Batrla et al. 1983; Stutzki et al. 1984). Toward DR 21, subsequent single-dish observations confirmed the anomalies seen in the HF components (see, e.g., Matsakis et al. 1980; Guilloteau et al. 1983). Specifically, the single-dish absorption spectrum shows the outer blueshifted and inner redshifted $NH_3$ (1, 1) HF components with stronger absorption than expected under conditions of LTE and the inner blueshifted HF component with less absorption than expected. The outer redshifted HF component is found in emission rather than absorption.

All previous studies of non-LTE effects in $NH_3$ have been conducted with a maximum spatial resolution of 40″. Use of this moderate spatial resolution presents some interesting problems for studies of DR 21, in which it is known that both $NH_3$ absorption (toward the H II region) and $NH_3$ emission (away from the H II region) occur within a 40″ region (Wilson et al. 1995). The mixing of emission and absorption makes analysis of the single-dish studies of anomalous absorption toward DR 21 difficult, at best. It is also known that in Orion $NH_3$ clumps exhibit size scales of order 1″ or smaller (see, e.g., Migenes et al. 1989). Thus it is possible (and actually shown in this Letter) that local excitation conditions vary considerably within the 40″ beam used in previous observations. Therefore, we have used the VLA to investigate in greater detail the non-LTE $NH_3$ (1, 1) absorption toward DR 21. The spatial resolution obtained is $\geq$20 times better than previous observations. One of the most unexpected and interesting results is that we have found that the LTE departure for the inner and outer $NH_3$ (1, 1) HF components is spatially anticorrelated. This indicates that a portion of the $NH_3$ (1, 1) gas seen toward the H II region is expanding while another portion is in collapse. Another unexpected result is the existence of a high brightness temperature, pointlike $NH_3$ maser feature located just to the southwest of the H II region continuum peak. This is the first example of an interstellar $NH_3$ (1, 1) maser. The flux density of the maser, found in the outer redshifted HF component, is more than 1.4 times greater than the absolute value of the flux density of the other HF components at this position, including the main line.

## 2. OBSERVATIONS AND RESULTS

The observations were made in a single session on 1992 September 17 with the VLA telescope of the NRAO.[4] At the time of these observations, the VLA was in the D configuration. Approximately 1.5 hr of the 6 hr session were spent observing DR 21 in the $NH_3$ (1, 1) transition. The observations were conducted in a spectral-line mode using a total bandwidth of 6.25 MHz separated into 63 Hanning-weighted channels, which provided a spectral resolution of 97 kHz (1.24

[1] US Naval Observatory, 3450 Massachusetts Avenue NW, Washington, DC 20392-5420.
[2] Max-Planck-Institut für Radioastronomie, Postfach 2024, D-53010 Bonn, Germany.
[3] Department of Astronomy, University of Illinois, Urbana, IL 61801.

[4] The NRAO is operated by Associated Universities, Inc., under cooperative agreement with the National Science Foundation.

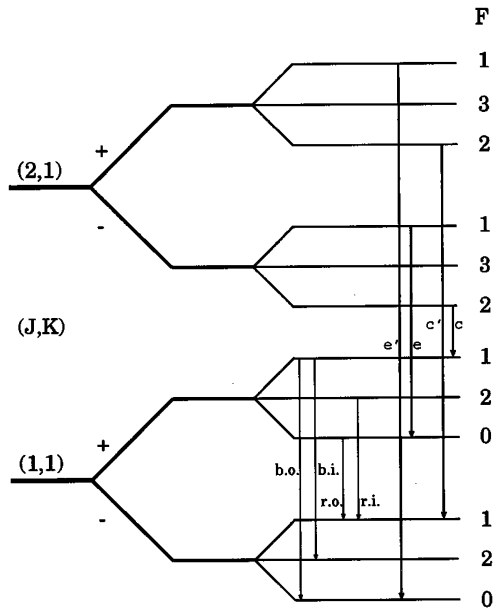


FIG. 1.—Energy-level schematic of the $(J, K) = (1, 1)$ and (2, 1) states of the $NH_3$ molecule. Splittings of the energy levels are not to scale. The blue- and redshifted inner and outer HF inversion transitions of the (1, 1) level are labeled as b.i., r.i., b.o., and r.o. Four IR rotational transitions between the (2, 1) and (1, 1) levels are labeled e, e′, c, and c′.

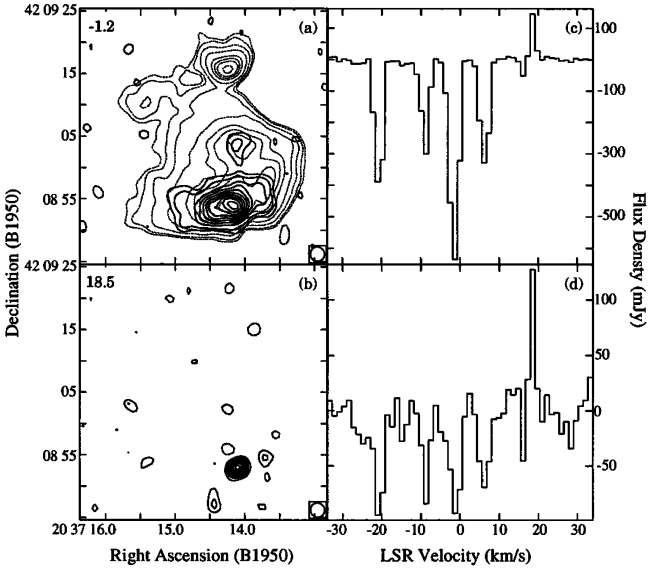


FIG. 2.—(*a*) Contour plot of the DR 21 continuum (*dashed contours*) and peak absorption channel ($-1.2$ km s$^{-1}$) of the $NH_3$ (1, 1) main HF component. Both contour plots have identical spatial resolution (2.″2). The FWHM beam is shown in the lower right corner of the plot. Contour levels of the continuum are $-2\%$, 2%, 3%, 6%, 12%, 25%, 35%, 45%, 65%, and 85% of 603 mJy beam$^{-1}$. Contour levels of the $NH_3$ (1, 1) absorption are $-6\%$, 6%, 12%, 25%, 35%, 45%, 55%, 65%, 75%, 85%, and 95% of $-431$ mJy beam$^{-1}$. (*b*) Contour plot of the $NH_3$ (1, 1) redshifted outer HF component with a spatial resolution of 2.″2. Contour levels are $-20\%$, 20%, 30%, 40%, 50%, 60%, 70%, 80%, and 90% of 130 mJy beam$^{-1}$. (*c*) Spectrum of the $NH_3$ (1, 1) transition at the position of the emission maximum of the redshifted outer HF component. This spectrum was derived from data with a spatial resolution of 3.″3. (*d*) Same as (*c*), but derived from data with a spatial resolution of 1.″7.

km s$^{-1}$). Channel 32 was set to an LSR velocity of 0 km s$^{-1}$. Source 3C 286 served as the absolute flux density calibrator, 2005+403 (2.4 Jy) as the phase calibrator, and 3C 84 as the bandpass calibrator. Data inspection and editing, flux, phase, and bandpass calibration, and subsequent processing and analysis were performed using the Astronomical Image Processing System (AIPS) software package of the NRAO. The wideband channel (channel 0) was self-calibrated, and the improved gain solutions applied to the spectral-line data set. To obtain "line-only" images, a linear fit to the continuum was performed and subtracted in the visibility plane using 19 channels without line emission or absorption. The data were Fourier-inverted using both natural and uniform weighting, using various subsets of the data to emphasize particular features. The resultant spatial resolution and rms noise in individual channel images varied over 3.″2–1.″7 and 6–20 mJy beam$^{-1}$, depending on the specific parameters chosen for the Fourier-transform step (e.g., $u$, $v$ weighting and range).

### 2.1. *The (1, 1) Line*

Both $NH_3$ (1, 1) emission and absorption are associated with the DR 21 H II region. The (1, 1) emission toward DR 21 is primarily localized in four clumps to the northeast, northwest, southeast, and southwest of the H II region. The characteristics of these emission regions and their relation to the H II region and powerful DR 21 molecular outflow are discussed in greater detail by Wilson et al. (1995). Absorption in the (1, 1) transition is found toward the H II region. A contour map of the strongest main HF component absorption channel (uniform weighting, 2.″3 resolution), projected on contours of the continuum, is shown in Figure 2*a*. The absorption region is clearly extended and is well resolved by the spatial resolution resultant from our observations.

Under conditions of LTE, the individual components of a satellite HF pair are expected to have equal intensity. However, this is *not* the case for the $NH_3$ (1, 1) absorption toward DR 21. In single-dish spectra of the (1, 1) absorption toward DR 21, the redshifted outermost HF component is found in emission, whereas absorption of the blueshifted outermost HF component is significantly deeper than expected under conditions of LTE (see Matsakis et al. 1980, Fig. 3; Guilloteau et al. 1983, Fig. 1). The opposite is observed for the inner HF components.

Lower resolution single-dish observations of $NH_3$ toward DR 21 average over the entire absorption region (and some of the emission region). Our interferometric observations, with 3″ resolution, are the first to resolve the DR 21 $NH_3$ (1, 1) absorption region. We find a significant degree of anomalous absorption toward the H II region. Figure 3 (Plate L4) shows the spatial distribution of the flux density ratios of the outer (Fig. 3*a*) and inner (Fig. 3*b*) pairs of HF components of the $NH_3$ (1, 1) level toward DR 21. The ratio data shown in Figure 3 were derived from the natural-weighted, 3.″2 resolution data since these have the highest signal-to-noise ratio. Under conditions of LTE, the ratio of these pairs of HF components is unity. Figure 3*a* depicts the flux density ratio of the outer redshifted to outer blueshifted HF components. Significant deviations from LTE are found across the entire absorption region. The most significant deviations are found southwest of continuum component C and against component B. At these positions the flux density ratio of the two outer HF components is negative since the redshifted component is found in emission and the blueshifted component in absorption. Figure

PLATE L4

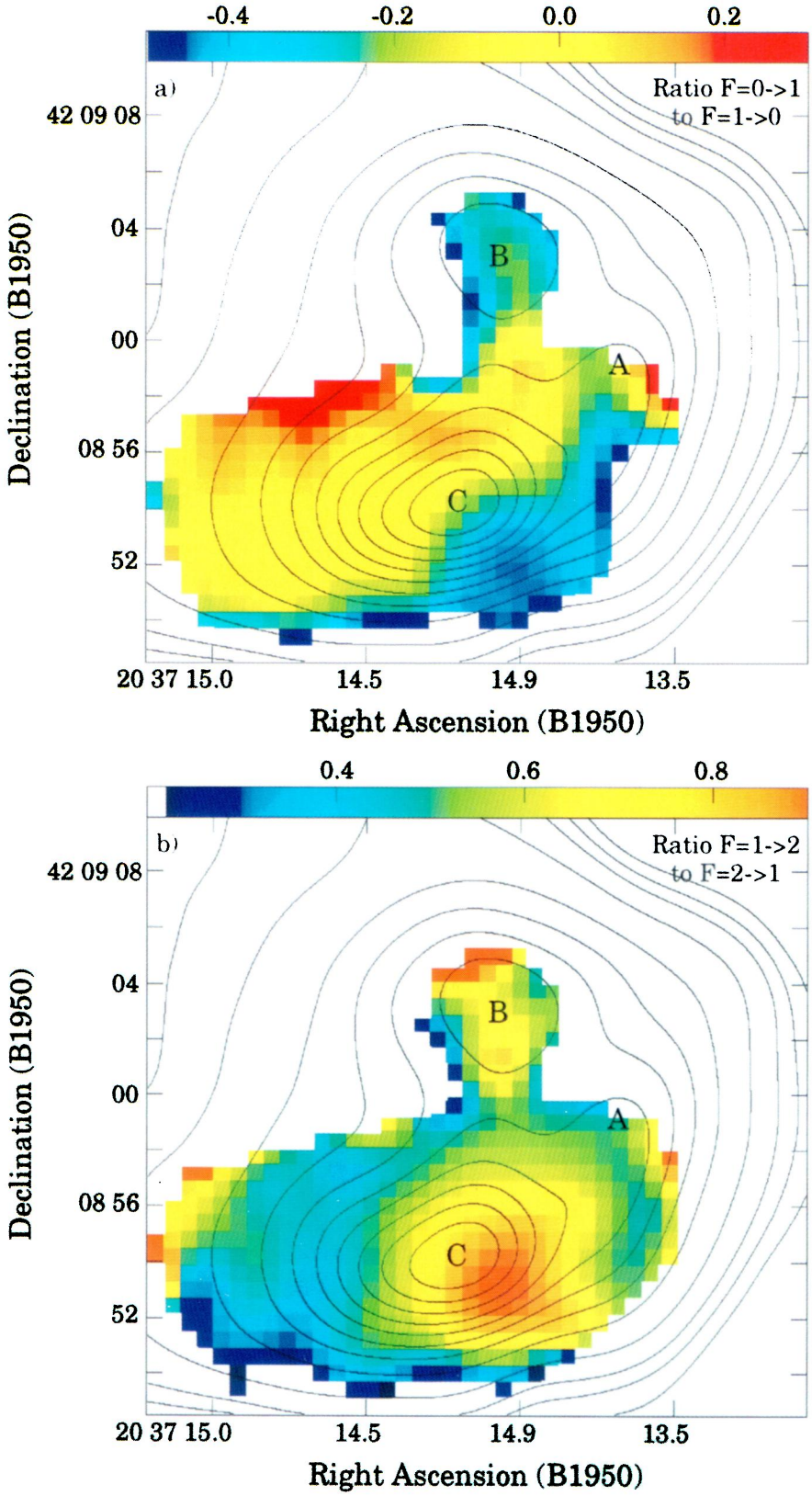


FIG. 3.—(*a*) Ratio of the flux density of the $NH_3$ (1, 1) redshifted outer HF component to the blueshifted outer HF component. (*b*) Ratio of the flux density of the blueshifted inner HF component to the redshifted inner HF component. Under conditions of LTE this ratio is 1. Note the spatial anticorrelation between the degree of LTE departure for the inner and outer HF components (see text). Contours of the DR 21 continuum are shown at 1.5%, 3%, 5%, 10%, 20%, 30%, 40% 50%, 60%, 70%, 80%, and 90% of the peak flux density of 1.2 Jy per 3″.3 × 3″.2 beam.

3*b* shows the flux density ratio of the inner blueshifted to inner redshifted HF components. The ratio closest to LTE is found southwest of continuum component C and against component B. Interestingly, the *inner* pair of HF components appears closest to LTE at the locations where the *outer* HF pair shows the greatest departure from LTE; i.e., the degree of departure from LTE for the inner and outer pairs of HF components is *spatially anticorrelated.*

The (1, 1) redshifted outer component is the only HF satellite component found in *emission* toward the H II region. The strongest emission is found southwest of continuum component C, near the position of the largest (1, 1) line-to-continuum absorption ratio (see Fig. 1 of Wilson et al. 1995). At this position a pointlike source of emission is found. A contour map of the peak channel (18.5 km $s^{-1}$) made with uniform weighting (2.″3 resolution) is shown in Figure 2*b*. A spectrum extracted at the peak position of this feature, derived from the highest S/N data, with 3″ spatial resolution (natural weighting), is shown in Figure 2*c*. To better determine the brightness temperature of the pointlike feature, we have created a higher spatial resolution image cube by excluding projected baselines shorter than 40 kλ and using uniform weighting in the Fourier-transform step. This procedure results in image data with a spatial resolution of ~1.″7. At this higher spatial resolution, the flux density of this emission feature is larger than the absolute value of the flux density of any of the other HF components (seen in absorption), including the main component! A spectrum derived from the 1.″7 data is shown in Figure 2*d*. A comparison of Figures 2*c* and 2*d* demonstrates the pointlike nature of the emission from the redshifted outer HF component. The flux density of the extended absorption region decreases in the higher spatial resolution spectrum by nearly a factor of 7, whereas the flux density of the pointlike outer redshifted HF component does not change significantly. A Gaussian fitting procedure shows that the emission feature is unresolved at this spatial resolution. Assuming an upper limit for the size of the emission feature of 0.″8 ($\frac{1}{2}$ beamwidth), the brightness temperature is $T_b > 600$ K. $NH_3$ rotation temperatures derived from nearby gas are considerably less (Wilson et al. 1995). Thus, based solely on our analysis of the brightness temperature, we conclude that a maser emission mechanism must be invoked to explain this emission feature. This is the first proven instance of an $NH_3$ (1, 1) interstellar maser.

Matsakis et al. (1977) presented a model for the anomalous $NH_3$ (1, 1) absorption toward DR 21 based on single-dish data with a spatial resolution of 1.′5. This model was also discussed by Stutzki & Winnewisser (1985). The infrared rotational transitions that link the (2, 1) and (1, 1) levels of $NH_3$ are separated by at most 0.66 km $s^{-1}$ (the most redshifted and blueshifted IR transitions are shown in Fig. 1). Under LTE conditions, these infrared transitions overlap in velocity, are trapped equally, and reshuffle the (1, 1) population levels completely so that no deviations from LTE are possible. However, if the effective line width for a particular $NH_3$ clump were comparable with the 0.6 km $s^{-1}$ splitting of the IR transitions, then the infrared lines at the high-frequency end (e and e′ of Fig. 1) and low-frequency end (c and c′ of Fig. 1) would experience less overlap. The net effect would be to raise the populations of the $F = 0$ $(J, K) = (1, 1)$ levels in the case of the e and e′ infrared transitions and the $F = 1$ (1, 1) levels in the case of the c and c′ transitions, the former causing the anomalies in the outer (1, 1) HF components, the latter in the inner HF components. The quantitative model of Matsakis et al. (1977) and the more detailed model of Stutzki & Winnewisser (1985) appear to adequately explain the lower spatial resolution observations. However, these models *do not* agree with the spatial anticorrelation we find for DR 21. Since the current study is the first to employ a spatial resolution significantly greater than 40″, it is difficult to draw general conclusions concerning whether or not the previous models will adequately explain higher spatial resolution observations of other regions of anomalous $NH_3$ emission. Regardless, focusing on the more detailed model of Stutzki & Winnewisser (1985), we find several limitations. (1) The model does not include the effects of absorption, a strong IR field (which likely exists in DR 21), or dynamic cloud motions (expansion or contraction). (2) The model predicts that the degree of LTE departure for the inner and outer HF components is correlated. That is, the model predicts that physical conditions resulting in increasing LTE departure for the outer HF components are also conditions of increasing LTE departure for the inner HF components. Our high spatial resolution data shows that exactly the opposite is occurring in DR 21 (see Fig. 3).

We suggest that the spatial anticorrelation of the LTE departure for the inner and outer HF components may be understood by considering a dynamic model. This is the result of the competing effect of both the far red- and blueshifted rotational IR transitions linking the (2, 1) to the (1, 1) levels (see Fig. 1). As discussed previously, the c and c′ (Fig. 1) IR transitions produce line anomalies in the inner pair of HF components, whereas the e and e′ transitions produce outer-pair anomalies. In an $NH_3$ cloud where portions of the $NH_3$ gas are approaching each other (blueshifted), the e and e′ IR transitions increasingly overlap with other IR transitions, driving the outer $NH_3$ (1, 1) HF pair of components toward LTE. In this case we see enhancement of the c and c′ IR transitions, which in turn drives the inner $NH_3$ (1, 1) HF pair away from LTE. Exactly the opposite occurs for redshifted gas; the inner (1, 1) HF components are driven toward LTE and the outer HF components away from LTE.

Within the context of DR 21, we propose the following scenario: Just to the southwest of the strongest continuum component (C), we find the most dense and massive $NH_3$ cloud (Wilson et al. 1995). Here the H II region is density-bound, and its expansion is greatly retarded by the molecular cloud (see, e.g., De Pree, Rodríguez, & Goss 1995). The dense molecular material in this cloud is falling toward the H II region–molecular cloud interface. Because of the collapse motion, the material closer to the interface is found at a higher (redshifted) velocity compared to material farther from the H II region. As discussed above, this velocity redshift between $NH_3$ molecules within the cloud results in an increased LTE departure for the outer HF satellite components while driving the inner HF components toward LTE. The opposite effect is suggested for the $NH_3$ gas to the west and northwest of continuum component C. Here the H II region is readily expanding, and molecular material nearer the H II region is being accelerated (blueshifted) into the molecular cloud. This results in increased departures from LTE for the inner HF satellite components while driving the outer HF components toward LTE. This qualitative model requires confirmation by quantitative calculations.

## 3. CONCLUSIONS

Results are presented of the first high spatial resolution investigation into the $NH_3$ (1, 1) HF component anomalies. Toward the DR 21 H II region, the LTE departure for the inner and outer pairs of HF components is spatially anticorrelated. Previous models predicted a spatial correlation. This unexpected result may be explained by a dynamic model involving infall in one portion of the $NH_3$ cloud and outflow of molecular material in another portion.

Four of the five $NH_3$ (1, 1) HF components are found in absorption toward the DR 21 H II region. The outer redshifted HF component is found in both emission and absorption toward different portions of the H II region. The peak emission of the outer redshifted HF component contains a pointlike feature located just southwest of the continuum maximum. With a minimum brightness temperature of $\geq$600 K, this feature is the first confirmed case of an interstellar maser in the $NH_3$ (1, 1) level.

The authors appreciate the helpful suggestions of an anonymous referee. Portions of this work were performed while T. L. W. was a G. A. Miller Visiting Professor at the University of Illinois.

## REFERENCES

Batrla, W., Wilson, T. L., Bastien, P., & Ruf, K. 1983, A&A, 128, 279
De Pree, C. G., Rodríguez, L. F, & Goss, W. M. 1995, Rev. Mexicana Astron. Astrofis., 31, 39
Guilloteau, S., Wilson, T. L., Martin, R. N., Batrla, W., & Pauls, T. A. 1983, A&A, 124, 322
Matsakis, D. N., Bologna, J. M., Schwartz, P. R., Cheung, A. C., & Townes, C. H. 1980, ApJ, 241, 655
Matsakis, D. N., Brandshaft, D., Chui, M. F., Cheung, A. C., Yngvesson, K. S., Cardiasmenos, A. G., Shanley, J. F., & Ho, P. T. P. 1977, ApJ, 214, L67
Migenes, V., Johnston, K. J., Pauls, T. A., & Wilson, T. L. 1989, ApJ, 347, 294
Stutzki, J., Jackson, J. M., Olberg, M., Barrett, A. H., & Winnewisser, G. 1984, A&A, 139, 258
Stutzki, J., Ungerechts, H., & Winnewisser, G. 1982, A&A, 111, 201
Stutzki, J., & Winnewisser, G. 1985, A&A, 144, 13
Townes, C. H., & Schawlow, A. L. 1955, Microwave Spectroscopy (New York: McGraw-Hill)
Wilson, T. L., Gaume, R. A., Johnston, K. J., & Tieftrunk, A. 1995, ApJ, 452, 693
Wilson, T. L., & Pauls, T. A. 1980, in IAU Symp. 87, Interstellar Molecules, ed. B. Andrew (Dordrecht: Reidel), 80